Liquid Drop Heating with Regard for Internal Circulation

Frolov S. M., Smetanyuk V. A.
N.N. Semenov Institute of Chemical Physics

Introduction

In two-phase flows and sprays, surface shear stresses between gas and liquid drops induce internal circulation of liquid [1, 2]. This effect is usually not taken into account in the majority of existing models of drop heating and gasification. It is believed that convective corrections to the heat transfer coefficient between gas and drop, like Ranz–Marshall correlation [3], compensate for the error caused by neglecting internal circulation. However, as shown in [2] this is not true: when applied to liquid drops, the correlations of Ranz-Marshall type obtained in wetted porous sphere experiments imply infinite thermal diffusivity of liquid, and therefore are not applicable at the initial transient period of drop heating. As shown in [4], for heavy hydrocarbon fuels like *n*-tetradecane, this period occupies up to 45%–50% of drop lifetime.

Internal circulation enhances heat transfer between surface and central regions of a liquid drop, and therefore affects the characteristic drop heating time. In addition to conductive mechanism of heat transfer, a convective mechanism comes into effect. As the hydrodynamic flow field inside a liquid drop becomes multidimensional, temperature distribution inside the drop may differ considerably from the classical spherically-symmetric distribution. Under such conditions, temperature sensitive properties of liquid drops can manifest themselves in a variety of phenomena. This paper deals with the analysis of temperature field in a moving liquid drop and a possible explanation of multicomponent drop 'microexplosion' phenomenon.

Problem Formulation

Consider a liquid drop in a uniform unconfined gaseous flow. From now on, drop and gas parameters will be denoted by indices *d* and *g*, respectively, and index 0 will label initial conditions. Initially, at $t = 0$ the drop is a sphere of radius R. It is heated uniformly to temperature T_{d0} and quiescent, i.e., the velocity of its center of mass is zero: $U_{d0} = 0$. The gas flow velocity is $U_g = U_{g0}$ and temperature $T_g > T_{d0}$. Due to velocity difference, $V_0 = U_g - U_{d0}$, the drop starts to move ($U_d \neq U_{d0}$ at $t > 0$) and deform under the action of aerodynamic forces. In addition, shear stress at the drop surface induces internal liquid circulation inside the drop. Due to temperature difference $\Delta T = T_g - T_{d0}$, heat transfer between gas and drop occurs resulting in drop heating and enhancement of liquid vaporization at the surface. Heat transfer is governed by relative velocity V, difference between temperatures T_g and T_d, as well as gas and liquid thermo-physical properties: latent heat of vaporization, Q, specific heats c_g and c_d, densities ρ_g and ρ_d, thermal conductivities λ_g and λ_d, and dynamic viscosities μ_g and μ_d. If one takes into account that velocity and temperature fields around and inside the drop are nonuniform and transient, the general solution of the problem requires consideration of the conjugate set of nonstationary three-dimensional fluid dynamics equations with a free boundary representing liquid–gas interface.

Below, the other approach to the problem is suggested. The objective is to reveal the role of internal circulation on drop heating. The following simplifying assumptions were adopted:

(1) liquid is incompressible;
(2) phase transition is absent;
(3) drop is not deformed;
(4) boundary layer on liquid side is laminar and flow in the drop core is the Hill's spherical vortex solution [1, 2];
(5) variation of flow field in the drop is quasi-stationary.

Assumptions (2) to (4) are justified for drops of heavy hydrocarbon fuels at low subcritical Weber numbers $\mathrm{We} = R\rho_g V^2/\sigma << 5–6$ (σ is the surface tension) and relatively low liquid Reynolds numbers $\mathrm{Re} = 2\rho_d U_i R/\mu_d$ (U_i is the liquid velocity at drop surface). Validity of

assumption (5) is justified by comparison of characteristic time for a drop to establish a steady internal motion, $\tau_s = \rho_d R^2 / \mu_d$, and characteristic time of drop motion as a whole τ_v, obtained from the equation of motion:

$$m_d \frac{dV}{dt} = -C_D A \frac{\rho_g V|V|}{2} \tag{1}$$

with initial condition $V(0) = V_0$. Here, m_d and A are the drop mass and mid-section area, and C_D is the drag coefficient. It follow from Eq. (1) that $\tau_v = \frac{8}{3C_D}\frac{\rho_d}{\rho_g}\frac{R}{|V|}$. The ratio of these times, $\frac{\tau_s}{\tau_v} = \frac{3C_D}{16}\frac{\mu_g}{\mu_d}\mathrm{Re}_g << 1$, where $\mathrm{Re}_g = 2R\rho_g|V|/\mu_g \le 100$ is the gas Reynolds number, and [1]

$$C_D = 12.69\,\mathrm{Re}_g^{-2/3} \tag{2}$$

The Hill's spherical vortex solution is given by

$$\begin{aligned} U_\theta &= U_i\left(1 - 2r^2/R^2\right)\sin\theta \\ U_r &= U_i\left(1 - r^2/R^2\right)\cos\theta \end{aligned} \tag{3}$$

where θ and r are the angular and radial coordinates shown in Fig.1a, and U_θ and U_r are the tangential and radial components of liquid velocity (azimuthal velocity $U_\varphi = 0$), see Fig. 1*b*.

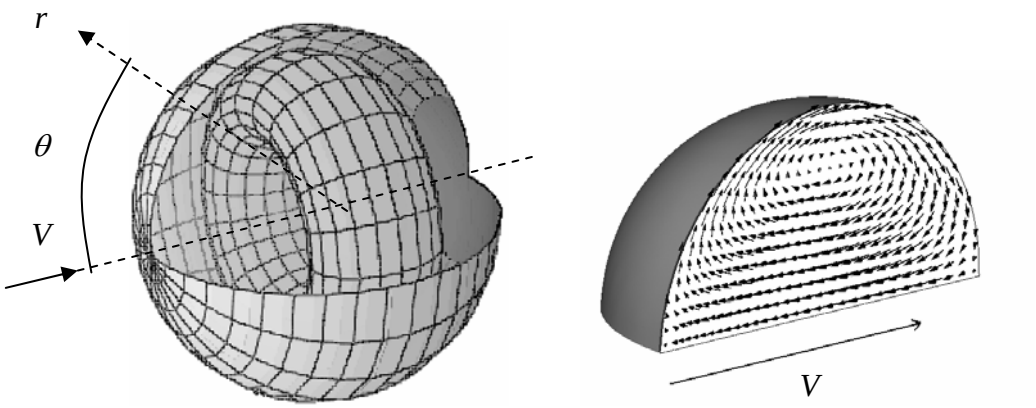

Figure 1: (*a*) Schematic of internal circulation and (*b*) predicted velocity field in liquid drop with indication of relative values of gas and liquid velocities

To determine velocity U_i one can use the Taylor's solution for interacting gas and liquid planar streams:

$$\begin{aligned} U(x,y) &= \alpha V \exp\left[-y/\left(\beta\sqrt{x}\right)\right] \\ U_i &= \alpha V \end{aligned} \tag{4}$$

where x and y are the longitudinal and transverse Cartesian coordinates and

$$\alpha = \left[\rho_g \mu_g / (\rho_d \mu_d)\right]^{1/3},\ \ \beta = \left[4\mu_d / (\alpha \rho_d V)\right]^{1/2}$$

The above assumptions simplify the problem. Drop heating is now governed by the equation of thermal conductivity

$$\frac{\partial T}{\partial t} + U_r \frac{\partial T}{\partial r} + \frac{U_\theta}{r}\frac{\partial T}{\partial \theta} = a\left[\frac{1}{r^2}\frac{\partial}{\partial r}\left(r^2 \frac{\partial T}{\partial r}\right) + \frac{1}{r^2 \sin\theta}\frac{\partial}{\partial \theta}\left(\sin\theta \frac{\partial T}{\partial \theta}\right)\right] \tag{5}$$

with the velocity field given by Eqs.(1)–(4). Here $a = \lambda/(\rho c_p)$ is the temperature diffusivity coefficient. Initially, $T(0, r, \theta) = T_{d0}$ was assumed everywhere except for the drop surface where $T(0, R, \theta) = T_{i0}$. To avoid solution of the conjugate problem, temperature $T_i = T(t, R, \theta)$ was treated as the constant parameter of the problem equal to T_{i0}.

The set of Eqs. (1)-(5) was represented in nondimensional form:

$$u_\theta = u_i\left(1-2\xi^2\right)\sin\theta$$

$$u_r = u_i\left(1-\xi^2\right)\cos\theta$$

$$u_i = \alpha v \qquad (6)$$

$$\frac{dv}{d\tau} = -\frac{3}{8}C_D\left(\frac{\rho_g}{\rho_d}\right)v^2$$

$$C_D = 12.69u_i^{-2/3}\,\mathrm{Re}_{g0}^{-2/3}$$

$$\frac{\partial \vartheta}{\partial \tau} + u_r\frac{\partial \vartheta}{\partial \xi} + \frac{u_\theta}{\xi}\frac{\partial \vartheta}{\partial \theta} = \frac{\omega}{\xi^2}\left[\frac{\partial}{\partial \xi}\xi^2\frac{\partial \vartheta}{\partial \xi} + \frac{1}{\sin\theta}\frac{\partial}{\partial \theta}\sin\theta\frac{\partial \vartheta}{\partial \theta}\right]$$

where

$$u = \frac{U}{\alpha V_0},\ v = \frac{V}{\alpha V_0},\ \xi = \frac{r}{R},\ \tau = \frac{\alpha V_0 t}{R},\ \vartheta = \frac{T}{T_{d0}},\ \vartheta_i = \frac{T_i}{T_{d0}},$$

$$\omega = \frac{a}{\alpha V_0 R},\ \mathrm{Re}_{g0} = \frac{2R\rho_g V_0}{\mu_g}$$

Initial and boundary conditions for Eqs. (6) are:

$$t = 0:\ v = \alpha^{-1},\ \vartheta(0 \le \xi < 1, \theta) = 1,\ \vartheta(\xi = 1, \theta) = \vartheta_i$$

$$t > 0:\ \vartheta(\xi = 1, \theta) = \vartheta_i;\ \left.\frac{\partial \vartheta}{\partial \theta}\right|_{\theta = 0, \pi} = 0$$

Thus the problem solution is governed by the following parameters: α, Re_{g0}, ρ_g/ρ_d, ϑ_i and ω. At specified thermo-physical parameters of gas and liquid (e.g., for the water–air system) the problem solution is governed by two parameters only: ϑ_i and ω, because relation $\mathrm{Re}_{g0}\,\omega = 2\rho_g a/\left(\alpha\mu_g\right)$ is a function of thermo-physical parameters too. Note that parameter ω is the ratio of characteristic drop heating times — convective $t_{conv} = R/(\alpha V_0)$ and conductive $t_{cond} = R^2/a$. Note also that $\omega = \infty$ corresponds to purely conductive heat transfer.

Results of Calculations

The problem was solved numerically for a drop quarter as shown in Fig. 1*b*. Figures 2 to 4 show different types of temperature distributions in water drops at ω = 0.1 (Fig. 2), 0.01 (Fig. 3) and 0.001 (Fig. 4) at surface temperature ϑ_i =1.243. At $\omega \sim$ 0.1 and larger, temperature distribution in the drop resembles that in the classical case with the minimal temperature always attained in the vicinity of the drop center. Nevertheless some displacement of temperature minimum toward the upwind drop side is visible in Fig. 2*c*. The heating mode with such a monotonous temperature distribution will be referred to as the conductive mode.

At $0.01 \sim \omega < 0.1$, temperature distribution in the drop becomes nonmonotonous (Fig. 3*a*). Minimal temperature is attained at a certain location between drop surface and drop center far from the axis of symmetry (Fig.3*b* and *c*). This location does not coincide with the vortex center. Contrary to the classical case, drop center exhibits a local temperature maximum. At the late

stage of drop heating, temperature in the drop center is comparable with the surface temperature, whereas the minimal temperature is relatively low. The heating mode with such a temperature distribution will be referred to as the conductive-convective or intermediate mode, because both mechanisms of heat transfer — conductive and convective — play a significant role in drop heating dynamics.

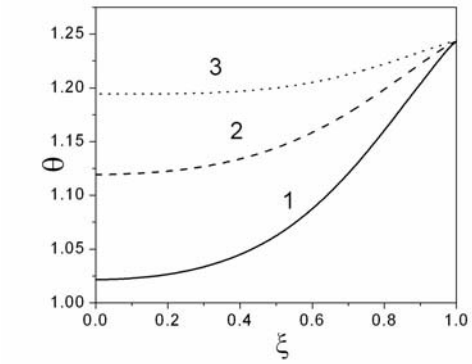

(*a*) (*b*) (*c*)

Figure 2: Predicted radial temperature distribution at $\tau = 4.86 \cdot 10^{-2}$ (*1*), $9.3 \cdot 10^{-2}$ (*2*), and $1.47 \cdot 10^{-1}$ (*3*) in the transverse drop cross-section (*a*) and in longitudinal cross-section at $\tau = 7.2 \cdot 10^{-2}$ (*b*), and $8.2 \cdot 10^{-2}$ (*c*). ω=0.1. Interval between isotherms is $\Delta\vartheta = (\vartheta_i - \vartheta_{\min})/10 = 0.024$

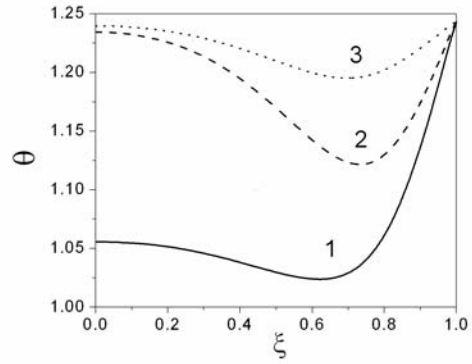

(*a*) (*b*) (*c*)

Figure 3: Predicted radial temperature distribution at $\tau = 1.38 \cdot 10^{-2}$ (*1*), $3.72 \cdot 10^{-2}$ (*2*), and $6.48 \cdot 10^{-2}$ (*3*) in the transverse drop cross-section (*a*) and in longitudinal cross-section at $\tau = 1.38 \cdot 10^{-2}$ (*b*), and $1.86 \cdot 10^{-2}$ (*c*). ω=0.01. Interval between isotherms is $\Delta\vartheta = (\vartheta_i - \vartheta_{\min})/10 = 0.024$

At $\omega < 0.01$, temperature distribution in the drop is also nonmonotonous (Fig. 4*a*). However, in contrast to Fig. 3, minimal temperature is attained at the vortex center during nearly the whole drop heating history (Fig.3*b* and *c*). In the drop center, a local temperature maximum exists with temperature values close to that at the drop surface. The heating mode with such a temperature distribution will be referred to as the convective mode, because isotherms become similar to velocity isolines.

Figure 5 shows the summary plot of the characteristic drop heating time vs. ω. The ratio $\tau_\eta^\omega / \tau_\eta^\infty$ indicates how the heating time at finite ω, τ_η^ω, differs from the classical heating time, τ_η^∞. Index $\eta = \dfrac{\vartheta_{\min} - 1}{\vartheta_i - 1}$ stands for indicating the heating degree. Computational curves for all heating degrees η lie in the strip bounded by broken curves, demonstrating intrinsic similarity of the heating process. Moreover, both dynamic solutions with variable *v* and static solutions with constant *v* hit in the domain bounded by the strip. As an example, two sets of dynamic solutions for different η are shown by symbols in Fig. 5.

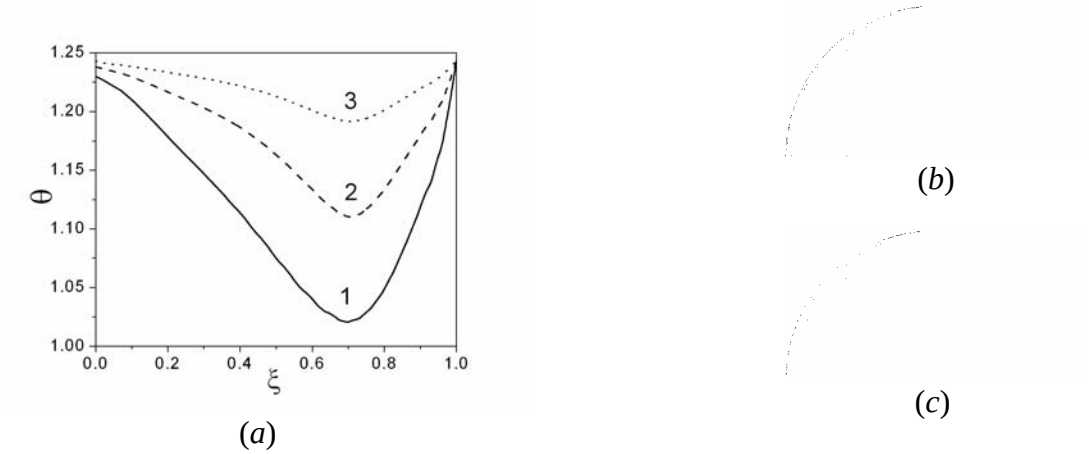

Figure 4: Predicted radial temperature distribution at $\tau = 1.38 \cdot 10^{-2}$ (*1*) , $3.72 \cdot 10^{-2}$ (*2*), and $6.48 \cdot 10^{-2}$ (*3*) in the transverse drop cross-section (*a*) and in longitudinal cross-section at $\tau = 1.38 \cdot 10^{-2}$ (*b*), and $1.86 \cdot 10^{-2}$ (*c*). ω=0.001. Interval between isotherms is $\Delta\vartheta = (\vartheta_i - \vartheta_{\min})/10 = 0.024$

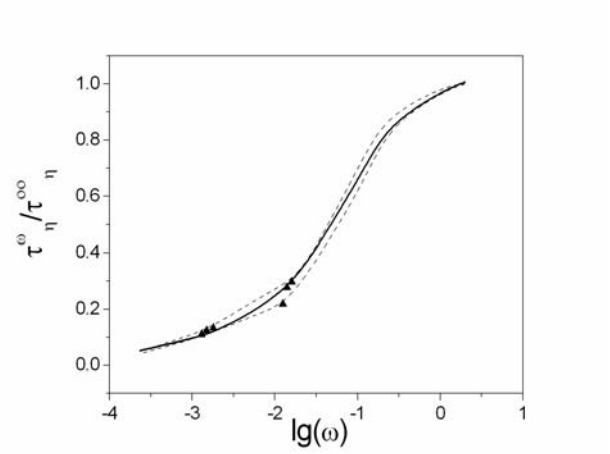

Figure 5: Predicted dependence of drop heating time on ω. The ratio $\tau_\eta^\omega / \tau_\eta^\infty$ indicates how the heating time at finite ω, τ_η^ω, differs from the classical heating time, τ_η^∞. Index $\eta = \dfrac{\vartheta_{\min} - 1}{\vartheta_i - 1}$ stands for indicating the heating degree. Computational curves for all heating degrees η lie in the strip bounded by broken curves, demonstrating intrinsic similarity of the heating process

The data in Fig. 5 can be approximated by the function shown by the solid curve. Using this function, one can readily estimate drop heating times with regard for internal circulation. For this purpose, one has to calculate drop heating time based on the standard solution of spherically

symmetric problem τ_η^∞ and multiply it by a factor $\tau_\eta^\omega / \tau_\eta^\infty$ at a given ω. This result is the first important outcome of the study. It follows from Fig. 5 that at $\omega < 0.2$ (i.e. in conductive-convective and convective modes of drop heating) the effect of internal circulation becomes considerable decreasing the heating time by more than 20%. At ω=0.01, the heating time is by a factor of 5 less than that provided by the classical model.

The other important outcome of the study is relevance of these findings to the problem of multicomponent drop 'microexplosion.' Let us assume that liquid consists of two components with essentially different volatilities. To make a qualitative analysis of the concentration (mass fraction) field $C(t,r,\theta)$ of the volatile component, one can solve the diffusion equation with the source term $\dot{r}$ describing the phase transition rate:

$$\frac{\partial C}{\partial t} + U_r \frac{\partial C}{\partial r} + \frac{U_\theta}{r}\frac{\partial C}{\partial \theta} = D\left[\frac{1}{r^2}\frac{\partial}{\partial r}\left(r^2 \frac{\partial C}{\partial r}\right) + \frac{1}{r^2 \sin\theta}\frac{\partial}{\partial \theta}\left(\sin\theta \frac{\partial C}{\partial \theta}\right)\right] + \dot{r} \qquad (6)$$

and with initial and boundary conditions:

$$t = 0:\ C(0 \le r \le R, \theta) = C_0 \le 1$$

$$t > 0:\ \left.\frac{\partial C}{\partial r}\right|_{r=R} = 0;\ \left.\frac{\partial C}{\partial \theta}\right|_{\theta=0,\pi} = 0 \qquad (7)$$

In Eqs. (6) and (7), D is the molecular diffusion coefficient, and C_0 is the initial mass fraction of volatile component. In general, phase transition rate $\dot{r}$ includes two contributions: one due to phase transition at nuclei formed according to homogeneous mechanism, $\dot{r}_f$, and the other due to phase transition at nuclei existing in liquid as impurity microparticles (and/or microbubbles), $\dot{r}_h$, i.e., $\dot{r} = \dot{r}_f + \dot{r}_h$. Rates $\dot{r}_f$ and $\dot{r}_h$ depend on liquid overheat $\Delta T = T - T_s$, where T_s is the saturation temperature at given pressure, on the number of spontaneously formed nuclei of supercritical size n_f, and on the number of impurity microparticles (and/or microbubbles) n_h. At $\Delta T \le 0$ and $C = C_0$ these rates are zero: $\dot{r}_f = 0$, $\dot{r}_h = 0$. At positive overheat, $\Delta T > 0$, vaporization of volatile component commences and rates $\dot{r}_f$ and $\dot{r}_h$ can be obtained from the relations:

$$\Delta T > 0: \quad \dot{r}_f = -a_1 C n_f, \quad \dot{r}_h = -a_2 C n_h \qquad (8)$$

Temperature decrease below T_s ($\Delta T < 0$) at $C < C_0$ will lead to changing the direction of phase transition from liquid vaporization to vapor condensation on the nuclei, i.e.,

$$C < C_0,\ \Delta T < 0: \quad \dot{r}_f = a_1 (C_0 - C) n_f, \quad \dot{r}_h = a_3 (C_0 - C) n_h \qquad (9)$$

In Eqs. (8), (9), a_1 and a_2 are the parameters depending on liquid properties and sizes of nuclei. The number of spontaneously formed nuclei n_f is related to overheat ΔT by the equation [5]:

$$n_f = a \exp\left[-\left(\frac{\Delta T_*}{\Delta T}\right)^2\right] \qquad (10)$$

where a and ΔT_* are the parameters depending on temperature T and liquid properties. The number of microparticles n_h depends on liquid purity. For solving Eq. (6), several simplifying assumptions were adopted: (i) it was assumed that phase transition does not affect drop heating, i.e., Eq. (6) was solved with the known temperature field in the passive scalar approximation; (ii) the concentration of impurities in liquid was assumed zero, n_h = 0, i.e., only homogeneous nucleation was taken into account; and (iii) variation of preexponential parameter $A = a_1 a$ in the relationship for $\dot{r}_f$ was neglected as compared to exponent. Under these assumptions, the rate of phase transition was taken in the form:

$$\dot{r} = \dot{r}_f \approx \begin{cases} 0 & at\ \Delta T < 0, C = C_0 \\ -AC\exp\left[-\left(\dfrac{\Delta T_*}{\Delta T}\right)^2\right] & at\ \Delta T > 0 \\ A(C_0 - C)\exp\left[-\left(\dfrac{\Delta T_*}{\Delta T}\right)^2\right] & at\ \Delta T < 0, C < C_0 \end{cases}$$

In particular test cases, the following model constants were applied: $C_0 = 1$, $A = 100$ 1/c, $\Delta T_* = 1$ K, and $T_s = 350$ K. Note that these numerical values were chosen for purposes of illustration and do not necessarily correspond to a particular liquid.

Figure 6 shows predicted distributions of vaporization rates in the drop at two subsequent time instants (*a*) and (*b*) at the late stage of drop heating with $\omega = 10^{-2}$. The corresponding temperature field is presented in Fig. 3. The relative value of phase transition rate is determined by hill height. It is seen that the maximum vaporization rate is attained around the vortex core. Vaporization rate at drop surface is small due to vanishing concentration C, whereas vaporization rate in the vortex core is small due to low temperature level.

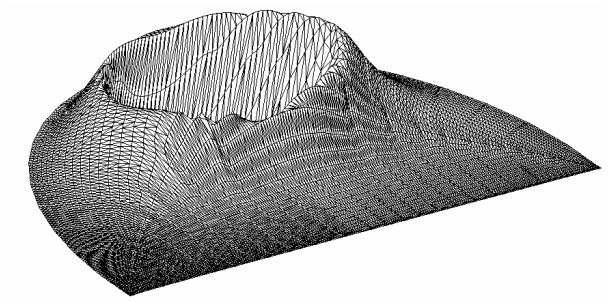

(*a*)

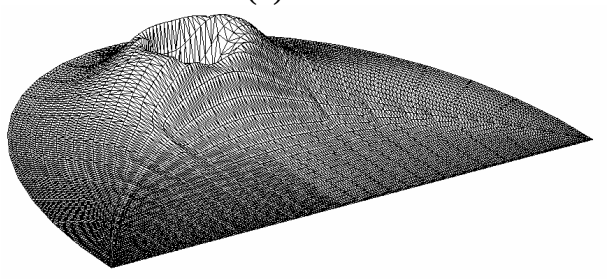

(*b*)

Figure 6: Predicted distributions of volumetric vaporization rates in the drop at two subsequent time instants (*a*) and (*b*) at the late stage of drop heating with $\omega = 10^{-2}$

Despite very approximate modeling, the results obtained may shed light on the formation mechanism of vapor bubbles in evaporating and burning multicomponent drops [6]. In experiments [6], formation of vapor bubbles in freely falling evaporating drops of 60% *n*-heptane + 40% *n*-hexadecane solution was observed. According to the observations, bubbles form in the region between drop center and drop surface. Figure 7 reproduces one of the photographs reported in [6] with two vapor bubbles formed in the drop.

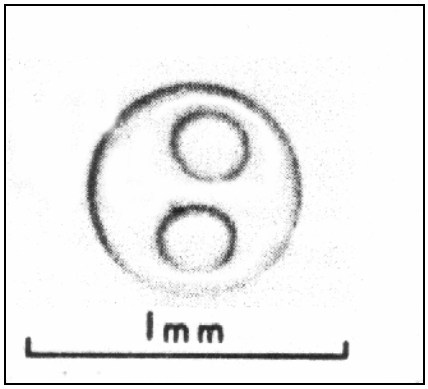

Figure 7: Photograph showing two vapor bubbles in the freely falling evaporating drop of 60% *n*-heptane + 40% *n*-hexadecane solution [5]

Concluding Remarks

Classical theory of liquid drop vaporization and combustion in gaseous flow does not take into account internal circulation of liquid induced by shear stresses on the gas–liquid interface. Arising convective flows in the form of toroidal vortices may affect dramatically heat and mass transfer between gas and liquid.

In the paper, transient calculations of liquid drop heating have been performed with regard for internal convective motion of liquid. At this stage of the study, aerodynamic deformation of liquid drops was not included in the analysis. It has been shown that depending on the Reynolds number of gas and drop relative motion there exist three characteristic modes of drop heating, namely, (1) conductive, (2) convective, and (3) intermediate. The conductive mode corresponds to the classical theory of drop heating. In the convective mode, drops are heated up considerably faster due to intense heat transfer from drop surface to drop center by means of votrical liquid motion. In the intermediate and convective modes, nonmonotonous radial temperature distributions with local temperature maximum in the drop center and local temperature minimum in the vortex center are realized. A simple approach for estimation of drop heating time with regard for internal circulation gas been proposed. A qualitative mechanism of vapor bubble formation in multicomponent liquid drops leading to drop ‘microexplosion’ has been suggested.

Acknowledgements

This work was supported by the Russian Foundation for Basic Research (grant No. 02-03-33168) and Federal Program ‘Integration’ (project A0030).

References

1. Abramzon B., Sirignano W. A. Droplet vaporization model for spray combustion calculations. J. Heat Mass Transfer, 1989, Vol. 32, No. 9, pp. 1605–1618.
2. Sirignano W. S. Fuel droplet vaporization and spray combustion theory. Prog. Energy Combust. Sci., 1983, Vol. 9, pp. 291–322.
3. Ranz W. E., Marshall W. R. Evaporation from drops. Chem. Engng. Prog., 1952, Vol. 48, pp. 141-146 and 173–180.
4. Frolov S. M., Posvianskii V. S., Basevich V. Ya. et al. Vaporization and combustion of hydrocarbon drop. II Nonempirical model of drop vaporization with regard for multicomponent diffusion. Rus. J. Chemical Physics., 2004, Vol. 23, No. 4, pp. 75–83.
5. Nigmatulin R. I. Dynamics of Multiphase Media. Moscow, Nauka Publ., 1987, Vol. 1, p.131.
6. Wang C. H., Liu X. Q., Law C. K. Combustion and microexplosion of freely falling multicomponent droplets. Combustion and Flame, 1984, Vol. 56, pp. 175–197.